

Studies of Supercapacitor Carbon Electrodes with High Pseudocapacitance

Yu.M. Volfkovich, A.A. Mikhailin,
D.A. Bograchev, V.E. Sosenkin and V.S. Bagotsky
*A. N. Frumkin Institute of Physical Chemistry and Electrochemistry,
Russian Academy of Sciences, Moscow,
Russia*

1. Introduction

During the last decades different new capacitor types were developed based on electrochemical processes. According to Conway [1] an electrochemical capacitor is a device in which different quasi-reversible electrochemical charging/discharging processes take place and for which the shape of the charging and discharging curves is almost linear, similarly to those in common electrostatic capacitors [1-13]. Electrochemical capacitors can be classified as film-type (dielectric), electrolytic and supercapacitors.

Electrolytic capacitors based on aluminium foils and liquid electrolytes are well-known for many decades. In them a thin film (thickness in the order of micrometers) of aluminum oxide prepared by electrochemically oxidizing the Al foils serves as dielectric film. Their specific energy is of the order of some hundredths Wh/L.

Electrochemical supercapacitors (ESCs) can be subdivided into electrical double-layer capacitors (EDLCs), pseudo-capacitors, and hybride-type capacitors. Historically the first ESCs which were developed were EDLCs. Up to now they remain the most important ESC version. The first prototypes of EDLCs were developed in the 1970s in Russia by N. Lidorenko and A. Ivanov [14] and also in Japan under the names "molecular energy accumulators" and "Ionistors".

The double-layer capacitor (EDLC) comprise two porous polarizable electrodes. The accumulation of energy in them proceeds through dividing positive and negative electrical charges between the two electrodes while maintaining a potential difference U between them. The electrical charge on each electrode depends on the electrical double-layer (EDL) capacity. Due to the very low thickness of this layer (tenths of a nanometer) the capacity value referred to unit of electrode's surface area is much higher than for electrolytic capacitors. Hence the term "*supercapacitor*" was introduced.

In order to achieve high capacity values in EDLCs highly dispersed carbonaceous electrodes with a high specific surface area of 1000-3000 m²/g are used, such as activated carbon (AC) or activated carbon cloths (ACC), nanofibers, nanotubes graphene sheets. The specific energy density of such capacitors reaches values of 1-20 Wh/L.

For a EDLSC with ideal polarizable electrodes the energy A delivered through a single discharge can be represented as:

$$A = (1/2) C [(U_{\max})^2 - (U_{\min})^2], \quad (1)$$

where C is the average electrode's capacity, and U_{\max} and U_{\min} are the initial, resp. the final values of discharge voltage. For full discharge until $U_{\min} = 0$ the maximal discharge energy will be: $A = A_{\max} = (1/2)C[(U_{\max})^2]$.

The development of EDLCs was induced by a necessity for rechargeable power sources with higher energy values, and power capabilities, and much better cyclability properties than those for existing storage batteries. Among the most remarkable features of EDLCs are excellent cyclability (hundred of thousands charge/discharge cycles as compared with hundreds of cycles for storage batteries) and the possibility to deliver for short periods high power and current densities, and also the possibility to be used at high and low temperatures (up to +60°C and down to -50°C). The cycling efficiency (ratio of energy consumed during charging and delivered during discharge) is about 92-95 %. Taking into account these properties, very promising are the following fields of applications for EDLCs: in ICE vehicles (in parallel with storage batteries) for starting purposes, delivering the necessary initial peak power (especially at low temperatures) and thus increasing the battery life time; and also in all-electric and in hybride vehicles for energy recuperation during slow-down and braking.

In *pseudocapacitors* electrical charges are accumulated mainly as the result of fairly reversible redox reactions (faradaic pseudo-capacity). Many such reactions are known in which oxides and sulfides of transition metals RuO_2 , IrO_2 , TiS_2 or their combinations take part.

One of the important achievements of modern electrochemistry is the development of *electron-conducting polymers*. Electrochemical reactions in systems with conjugated double bonds such as polyanilin, polythiophene, polypyrrolle, polyacethylene and others, are reversible and can be used in supercapacitors. Such processes are called electrochemical doping or dedoping the polymers with anions and cations. The electron conductivity during doping is due to the formation of delocalized electrons or electron-holes and their migration in the system of polyconjugated double-bonds under the influence of an applied electrical field. The use of some electron-conducting polymers as supercapacitor electrodes is based on the high reversibility of doping and dedoping reactions and the high conductance values of such polymers. The specific energy values of pseudocapacitors are fairly high 10-50 Wh/L and their cyclability reaches hundred thousands cycles. A disadvantage of supercapacitors based on transition metal oxides and sulfides is their high price. A disadvantage of those based on electron-conducting polymers is their insufficient stability.

Recently some *hybride-type supercapacitors* were developed in which different types of electrodes are used. In [15-18] capacitors were investigated in which the positive electrodes were based on metal oxides, and the negative electrodes on activated carbon (e.g. the system $NiOOH/KOH/AC$ or the system $PbO_2/H_2SO_4/AC$. In both of these two systems as positive electrodes conventional electrodes from alkaline, resp. lead-acid storage batteries are used. An advantage of the hybride-type supercapacitors as compared with their analogues, with symmetrical AC, is their higher U_{\max} value and correspondingly their

higher specific energy (up to 10-20 Wh/kg). The lower U_{\max} value for symmetric AC systems in comparison with the hybrid versions is due to the fact that at not very high anodic potentials (0.9-1.0 V) an oxidative carbon corrosion is observed while hydrogen evolution potential on the hybrid's negative AC electrode remains at very negative values up to -0.8 V). An advantage of hybrid supercapacitors over the corresponding storage batteries is the much higher cycling capability, and the possibilities of faster charging and of easier hermetically sealing. Hybrid $\text{PbO}_2/\text{H}_2\text{SO}_4/\text{AC}$ capacitors are used in wheelchairs and in electrical motor-buses.

In [19] a hybrid supercapacitor with a RuO_2 positive electrode and an AC negative electrode was described. A high specific energy of 26.7 Wh/kg was reported.

An important feature of supercapacitors in comparison with storage batteries is the possibility of rapid charging and discharging in very broad time intervals ranging from less than one second to several hours. Correspondingly supercapacitors can be subdivided into power units with high values of specific power and into energy units with high specific energy values.

Power supercapacitors allow carrying out the charging and discharging processes in very short time periods (from fractions of a second to minutes) and obtaining herewith high power characteristics from 1 to 5 kW/kg in concentrated aqueous solutions with high specific conductivity. Measurements for highly dispersed carbon electrodes in the energy capacitor operation modes usually yield the specific charge values in the range of 40 to 200 C/g [20, 21]. In the case of carbon materials, the limiting capacity obtained in [22] was 320 F/g due to a considerable contribution of pseudocapacitance of reversible surface group redox reactions (thus, they are not pure EDLCs anymore). In [23] high power characteristics (above 20 kW/kg) were obtained for electrodes based on single-wall carbon nanotubes (SWCNT). Such high power values can be explained by the regularity of the SWCNT's pore structure. As can be seen from Fig. 1 representing a SEM picture of this material, the pores are neither corrugated nor curving, thus providing for a high conductivity and, therefore, for a high power.

The electrodes used in energy-type ECSCs are often electrodes on which rather reversible faradaic processes occur. Such electrodes include electrodes based on electron-conducting polymers (polyaniline, polythiophene, polypyrrole etc.) and also electrodes based on some oxides of variable-valency metals (oxides of ruthenium, iridium, tungsten, molybdenum, zirconium etc.) [1, 2]. These electrodes feature different limitations for practical application, such as expensiveness, insufficient cyclability due to degradation processes etc. Using nonaqueous electrolytes in ECSC with electrodes based on highly dispersed carbon materials allows obtaining high (up to 3-3.5 V) charging voltage values, which significantly enhances the energy but limits the power of capacitors due to low conductivity of these electrolytes [1, 2, 24]. Aqueous alkali solutions allow obtaining rather high power values, but the low operating voltage range (about 0.8 V) decreases the energy characteristics of ECSC. Aqueous electrolytes with the highest conductivity are sulfuric acid solutions with concentrations from 30 to 40 wt. %. Besides, the working voltage range in the region of reversible processes proves to be above 1 V due to the relatively low corrosion activity towards carbon as compared to other aqueous electrolytes.

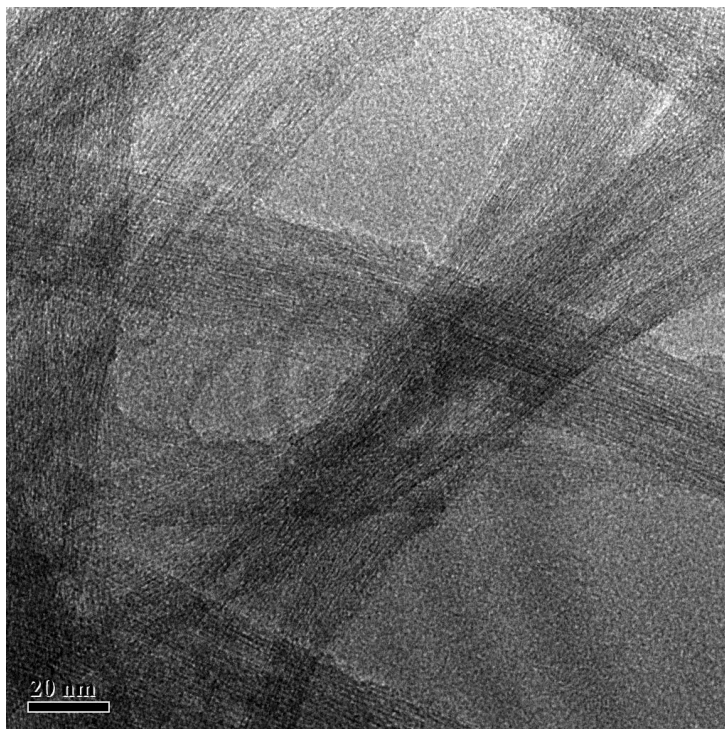


Fig. 1. SEM image of single-wall carbon nanotubes (SWCNT)

In [25], a very high maximum amount of electricity of 1150 C/g was obtained with electrodes based on ADG type activated carbon with the specific surface area of 1500 m²/g. This value was reached after deep cathodic charging to the potentials of -0.3 to -0.8 V RHE. On the basis of these data and on the basis of other various experiments it was assumed that such a high amount of electricity is obtained as a result of hydrogen intercalation into AC carbon limited by solid-phase diffusion. These experiments are as follows: a very slow (20 h and more) deep charging process, memory effect under potential scanning in the positive direction, absence of correlation between the specific surface area and specific capacitance values, linear dependence of current maximums on the square root of the potential sweep rate, and some other experimental data. It was concluded in this paper that the most probable limiting amount of electricity is that corresponding to the formation of a compound C₆H similar to the compound of C₆Li for negative carbon electrodes in rechargeable lithium-ion cells. However that formation of the C₆H compound according to Faraday's law requires consumption of 1320 C/g that was not obtained in [25].

Therefore, the aim of the present investigation was to reach the maximum possible capacitance values on AC and also a more detailed study of mechanisms of the processes occurring under deep cathodic charging. Besides that, the aim of the investigation was to develop a mathematical model of these processes and to compare it with experimental data.

There are only few papers on mathematic modeling of processes in ECSC. In [26], an EDLC model was developed taking into account EDL charging, potential distribution in a porous electrode due to ohmic energy losses and its porous structure. The calculation results agreed well with experimental galvanostatic charging–discharge curves. In [27, 28] an operation theory was developed for electrodes based on electron-conducting polymers used in supercapacitors. The theory takes into account EDL charging, potential distribution in a porous electrode, electrochemical kinetics, intercalation of counterions in the polymer phase, and a nonsteady-state solid-phase diffusion of counterions in this phase. Simulation of the experimental discharge curves allowed obtaining the values of the parameters of processes occurring in the electrode: the solid-phase diffusion coefficient, EDL specific capacitance, and exchange current density of the electrochemical reaction. In [29], a model of a SWCNT electrode was developed taking into account EDL charging, hydrogen electroadsorption-desorption, and kinetics of hydrogen electrooxidation–electroreduction according to the Volmer theory. In [30] an AC-based electrode impedance model accounted for EDL charging and intercalation processes, using statistical thermodynamics. However, in [29, 30] there was no comparison between the theory and experiment

2. Experimental methods

The following electrochemical methods were used in this work: cyclic voltammetry, galvanostatic, and impedance techniques. The electrochemical impedance spectra were obtained using an electrochemical measurement system consisting of a Solartron 1255 frequency analyzer, Solartron 1286 potentiostat, and a computer, and also using a FRA impedance meter. Measurement of CVs and galvanostatic curves was carried out using Solartron 1286 and PI-50 potentiostats. Prolonged cell cycling was achieved using a Zaryad 8k cycling device. Apart from the impedance technique, the dc charged electrode resistance was measured as follows. After deep anodic charging, the cell for charging was disassembled and the working electrode was removed. Further, in order to remove the acid residue, the electrode was dried in contact with microporous acidproof filter paper. Then it was placed into a special four-electrode measurement cell and pressed between two liners of foil of thermally expanded graphite (TEG); copper disks with copper current leads were placed on the rear sides of this set. Further, the cell was sealed and the dependence of voltage on current was measured, from which the electrode resistance was calculated. An important feature of the method is that the cell with copper current leads must be assembled in a predetermined period of time (in our case, 3 min), as a deeply charged electrode undergoes gradual oxidation in air. An advantage of this method over impedance analysis is that it allows eliminating the polarization contribution into resistance as in the case of the impedance technique. Due to these limitations, both of these methods were used.

The main electrochemical measurements were carried out in a specially designed teflon filter-press cell with carbon current leads that allowed performing studies in a wide range of potentials. Its scheme is shown in Fig. 2,a and its photograph is presented in Fig. 2,b. Fig. 3 shows schematically the electrochemical group of this cell representing a matrix system, in which the electrolyte is in the pores of the electrode and separator. The separator is clamped between two ring-shaped acidproof rubber gaskets that are chosen depending on the

electrode thickness to provide reliable separation of the working and auxiliary electrodes. A fine-texture Grace-type separator (polyethylene with silica gel) was used in the cell. The capacitance of the AC auxiliary electrode was much higher than that of the working electrode, which allowed eliminating interaction of electrodes through the evolved gas. Application of graphite current leads instead of the usual metallic (most often, platinum) ones allowed reaching high negative potentials (up to -1 V RHE), which in its turn allowed obtaining ultrahigh capacitance values (see below).

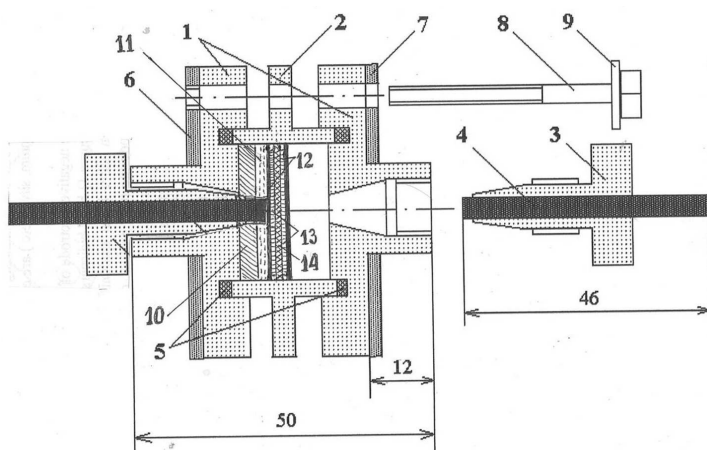


Fig. 2.a Electrochemical cell. The principal details: 4 – a graphite current lead, 12 – current distribution layer of thermal expanded graphite, 13 – electrodes, 14 – separator.



Fig. 2.b Photograph of the electrochemical cell

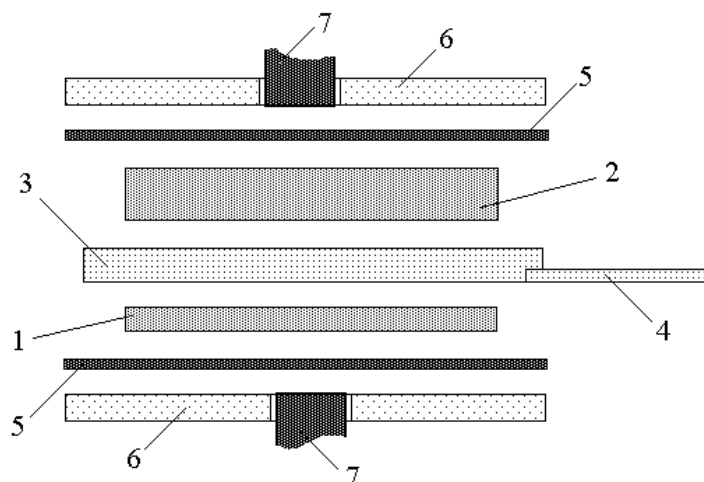


Fig. 3. Electrochemical group of the Teflon cell.

The electrolyte used in this study was mainly concentrated sulfuric acid with concentrations from 30 to 60%. The electrode used was a CH900-20 activated carbon cloth (ACC) (Japan). The electrodes had a surface area of 3 cm^2 , a thickness (in the compact state under the pressure of 0.5 MPa) of about 0.4 mm, and a mass of about 0.06 g.

Studies of the porous structure and hydrophilic-hydrophobic AC properties were carried out using the method of standard contact porosimetry (MSCP) technique [32] with evaporation of octane and water. The method is based on the laws of capillary equilibrium. If two (or more) porous bodies partially filled with a wetting liquid are in capillary equilibrium, the values of the liquid's capillary pressure in these bodies are equal. The value of the capillary pressure according to the Laplace equation is $p^c = 2\sigma \cos\theta/r$, where r - is the pore radius, σ - the surface tension, θ - the wetting angle. In this method the amount of a wetting liquid in the test sample (V_t) is measured; Simultaneously, the amount of the same wetting liquid (V_s) is measured in a standard specimen of known porous structure. The liquids in both porous samples are kept in contact. After some time a thermodynamic equilibrium is reached. The measurements are performed for different overall amounts of the liquid $V_0 = V_s + V_t$. During the experiment this overall amount is changed by gradual evaporation of the liquid. The MSCP with appropriate standard samples can be used to measure pore sizes in the range from 1 to $3 \cdot 10^5 \text{ nm}$. The MSCP has several substantial advantages over mercury porosimetry and other porosimetric methods. It has the possibility:

- to investigate materials with low mechanical strength (for example clothes), frail materials and even powders;
- to measure samples at fixed levels of compression and/or temperature, i.e., under conditions in which they are commonly used in different devices;
- to use for measurements the same liquid (for example water or aqueous solutions) as that, used in real devices (i.e. leading to the same swelling degree of the sample);
- no use toxic materials such as mercury.

One of the most pronounced advantages of the MSCP is the possibility to investigate the wetting (hydrophilic/hydrophobic or liophilic/liophobic) properties of porous materials. Primarily, the MSCP measures the distribution of pore volume vs. the capillary pressure p^c , i.e. vs. the parameter $r^* = r / \cos \theta$ (henceforth, this parameter is called effective pore radius). For partially hydrophobic materials (for which $\theta > 0$) the porosimetric curves measured with water are shifted towards higher values of r^* with respect to the curves measured with octane that wets most materials almost ideally ($\theta = 0^\circ$). The value of this shift for a certain value of pore volume V_n and of the corresponding pore radius r_n allows to determine the wetting angle of water for pores with the radius r_n :

$$\cos \theta = r_n / r^* \quad (2)$$

For porous materials the wetting angles $\theta(r)$ for pores of different size can be different.

3. Experimental results and discussion

Fig. 4 presents integral pore radius distribution curves measured using MSCP with octane and water for the CH900-20 AC cloth. As follows from this figure, this cloth has a very wide pore spectrum: from micropores with radii $r \leq 1$ nm to macropores with $r > 100 \mu\text{m}$, i.e. in the range of more than 5 orders of magnitude. It is of interest that this cloth contains micropores and also macropores with $r > 1 \mu\text{m}$, but there are practically no mesopores with $1 \text{ nm} < r < 100 \text{ nm}$. Micropores provide high full specific surface with $S_f = 1520 \text{ m}^2/\text{g}$ and hydrophilic specific surface $S_{\text{phi}} = 870 \text{ m}^2/\text{g}$. According to [32], porosimetric curves are measured using octane for all pores and using water only for hydrophilic pores. As follows from these curves, the full porosity (by octane) was 86%, the hydrophilic porosity was 78.5%, and the hydrophobic porosity was 7.5 %.

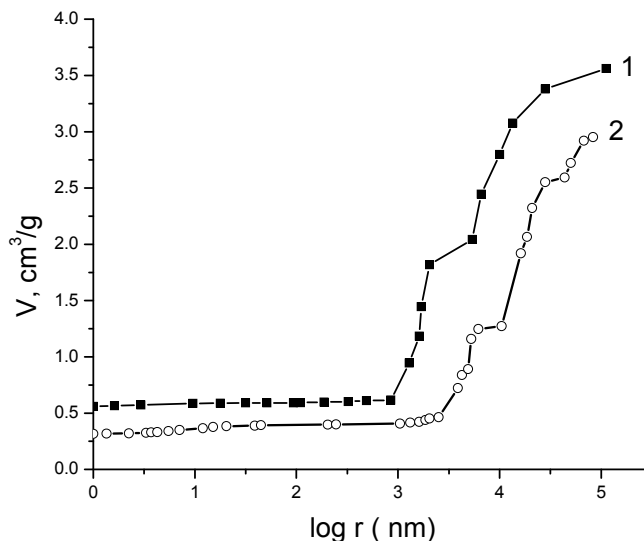


Fig. 4. Integral pore radius distribution curves measured in octane (1) and water (2) for a CH900-20 AC cloth.

Fig. 5 presents the dependence of the wetting angle θ on the pore radius calculated from Fig. 5 according to [32]. As may be seen, the θ values for the whole pore radius range are close to 90° . Therefore, though most of the pores are hydrophilic with $\theta < 90^\circ$, they are still badly wetted. This and also the presence of fully hydrophobic pores may point to high amounts of graphite (graphene) impurities that are practically hydrophobic. The complex curve character in Fig. 5 is largely due to a nonuniform distribution of surface groups in the pores of different radii.

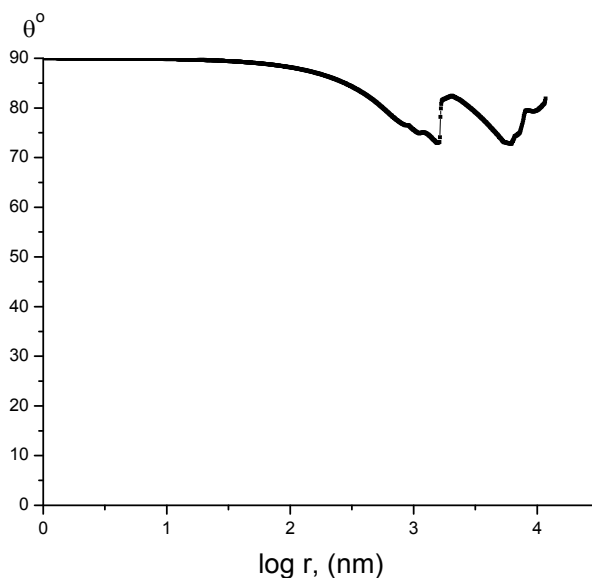


Fig. 5. Dependence of wetting angle θ on the pore radius for the CH900-20 AC cloth.

In this work, studies of AC were carried out in a large range of potentials from -0.8 to 1.0 V RHE. It is convenient to present the CV (especially those measured at different potential sweep rates w), graphically in the form of capacitance-voltage curves constructed in the coordinates of differential capacitance (C) vs. potential (E), where $C = dQ/d\tau = I d\tau / dE = I/w$, I is the current, Q is the amount of electricity, $w = dE/d\tau$, τ is the time.

Fig. 6 compares the cyclic capacitance-voltage curves measured in 48.5% H_2SO_4 at different potential sweep rates in two ranges of potentials: in the reversibility range (from 0.1 to 0.9 V) and in the deep charging range (from -0.8 to 1 V). As follows from curve 4 measured in the reversibility range, only electric double layer (EDL) charging occurs here, while pseudocapacitance of redox reactions of surface groups is very low in this case. This distinguishes the CH900-20 ACC from ADG AC in which a considerable contribution is introduced by the pseudocapacitance of fast redox reactions of surface groups [25]. As follows from curve 4, the value of the EDL capacitance is approximately 160 F/g. Taking into account that $S_{\text{phi}} = 870$ m^2/g , we obtain $C_{\text{DEL}} = 18.4$ $\mu\text{F}/\text{cm}^2$ for unit of the true hydrophilic carbon surface area. This value is close to the classical EDL capacitance value of platinum [33]. Much lower C_{EDL} values presented in [34], in our opinion, are explained by the fact that the values of the full specific surface area measured using the BET

technique were used, while it is known that carbon materials have both hydrophilic and hydrophobic pores. The MSCP used in this work allows to obtain the values of the hydrophilic surface area S_{phi} and thus the C_{DEL} values per unit of the real working surface area.

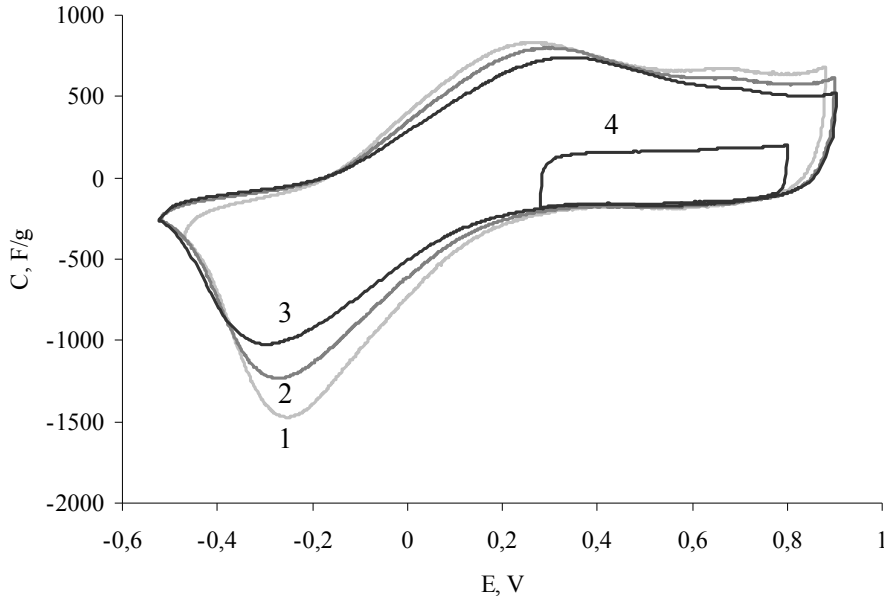


Fig. 6. Capacitance-voltage cyclic curves for CH900-20.

In the range of negative potentials (< -0.1 V) (curves 1, 2, 3), faradaic processes with a very high pseudocapacitance are observed. As may be seen, the EDL capacitance decreases in the range of negative potentials. This is probably due to the partial surface blocking by adsorbed particles. There are two pronounced maximums in the anodic branches of curves 2, 3 measured at low w values, which points to the probable occurrence of two slow processes. There is a single deep maximum corresponding to a very high amount of electricity under deep cathodic charging of AC in catodic branches of curves 1, 2, 3.

The method of galvanostatic curves was used to measure the amounts of electricity after long-term charging at negative potentials. Fig. 7 presents the dependence of the amount of electricity Q under discharge on the charging time at potential $E = -250$ mV in 40.3% H_2SO_4 . As may be seen, the Q value grows very fast at very low charging times of seconds and minutes and continues increasing further for many tens of hours. Such very slow growth can be explained by a very slow diffusion in a solid phase. Therefore it is possible to assume the existence of a hydrogen intercalation into AC carbon controlled by slow solid-phase hydrogen diffusion. This is also evidenced by a proportionality of the limiting current to the square root of the potential sweep rate and also by a number of other experimental data obtained in [25] (memory effect under potential sweep in the positive direction, absence of correlation between the specific surface area value and specific capacitance etc.) It was

assumed in [25] that during a deep cathodic charging of AC, as a result of hydrogen intercalation a compound C_xH and in the limiting case C_6H is formed. On the basis of the shape of the potentiodynamic curves it is also possible to assume that two processes take place: a fast hydrogen chemisorption at the interface of carbon and electrolyte in the pores and a process of hydrogen intercalation into AC with a slow hydrogen solid-phase diffusion.

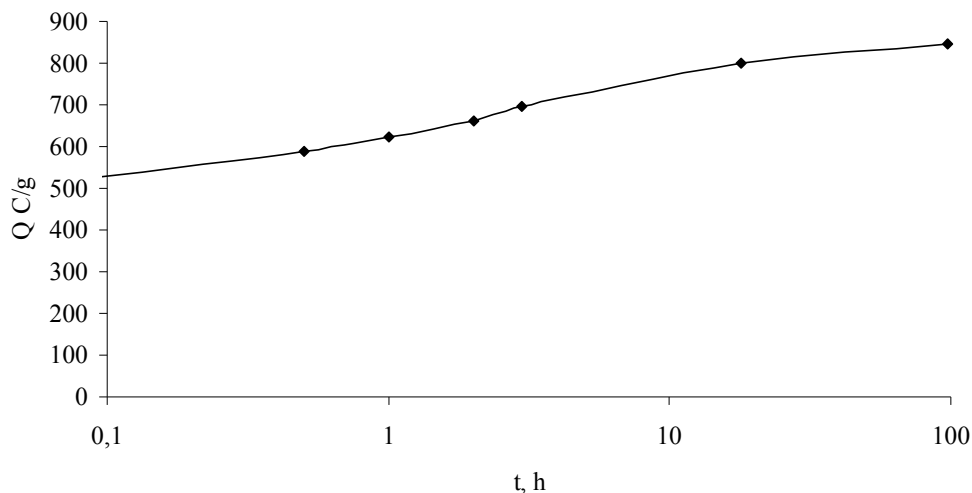


Fig. 7. Dependence of specific amount of electricity under discharge of the CH900-20 electrode in 40.3% sulfuric acid on the charging time under the charging potential of -250 mV.

Fig. 8 presents the dependence of the active resistance of the electrode on charging time at $E = -400$ mV measured using the impedance technique in 40% sulfuric acid. As can be seen, the active resistance of the electrode grows in the course of the charging process. Both the solid phase and electrolyte in pores contribute to the resistance. The dependence of electric resistance on the charging time measured under constant current according to the above mentioned technique is more significant. Fig. 9 presents such a dependence of the dc resistance of a CH900-20 electrode on the charging time in 40.3% sulfuric acid at $E = -0.34$ V. As seen from this figure, the electrode resistance grows significantly with an increase in the AC charging time. One should keep in mind that the above parameters were obtained on activated carbon cloth (CH900-20), which practically eliminates the effect of contact resistance between its separate fibers, as the fibers represent practically parallel transport paths for electrons. Therefore, the above data may be explained by a change in the bulk phase chemical composition in the course of charging. Thus, both resistance measurement techniques point to its increase as dependent on the charging time. This can also be explained by a change in the solid phase composition: from C to C_xH and, in the limit, to C_6H .

The maximum specific charge of 1560 C/g was obtained after charging for 22 h at the potential of $E = -0.31$ V RHE in 56.4% H_2SO_4 . No close value was described in the literature

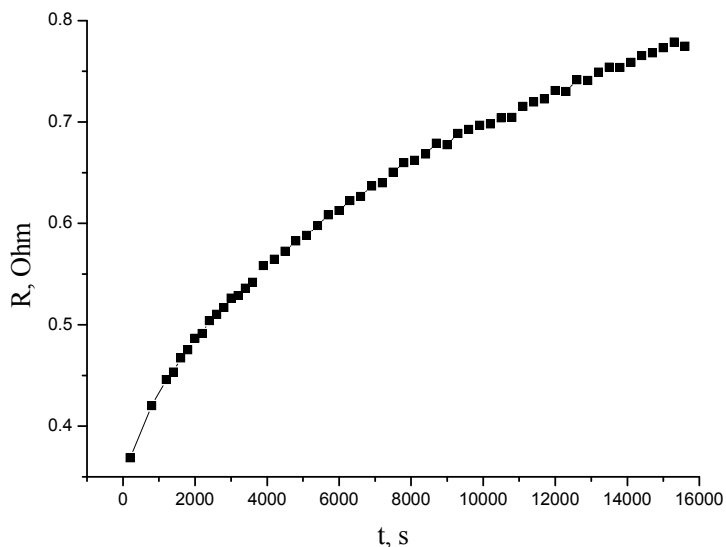


Fig. 8. Dependence of active resistance of the electrode on the charging time at $E = -400$ mV measured using the impedance technique in 40% sulfuric acid.

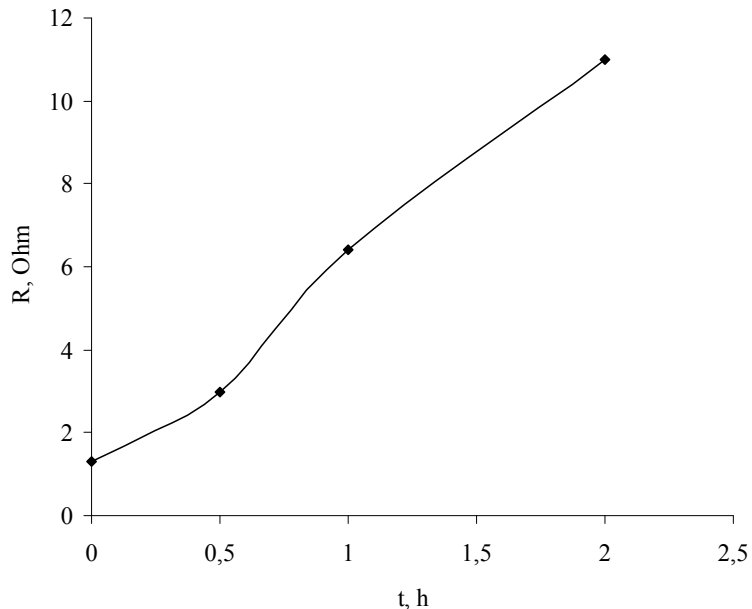


Fig. 9. Dependence of electron resistance of the CH900-20 electrode on the charging time in 40.3 % sulfuric acid at $E = -0.34$ V measured under constant current.

Fig. 10 presents the dependence of the maximum specific charge of CH900-20 on the sulfuric acid concentration (in the range from 34 to 56%) for the discharge time of 18 h. As follows from this figure, the specific charge grows with an increase in the sulfuric acid concentration. The following explanation is possible: It is known from the literature that: 1) in concentrated sulfuric acid solutions a sulfuric acid intercalation occurs into graphite and graphite-like materials, that is enhanced at an increase in the concentration [35–37]. During this intercalation the gap between graphene layers where the acid penetrates grows. 2) Activated carbons to a certain degree are swelling during adsorption of different adsorptives [38]. As graphite-like impurities are contained in AC [39, 40]. Taking into account these facts, it is possible to assume that in the described conditions a **double intercalation** occurs. Sulfuric acid is intercalated into AC expanding the interlayer (intergraphene) space. Hydrogen atoms are then directed into this space under deep cathodic charging of AC. This interlayer space serves as a transport route for hydrogen. Then hydrogen interacts with the graphene layers with the ultimate formation of compound C_6H (carbon hydride or hydrogen carbide) (see Fig. 11).

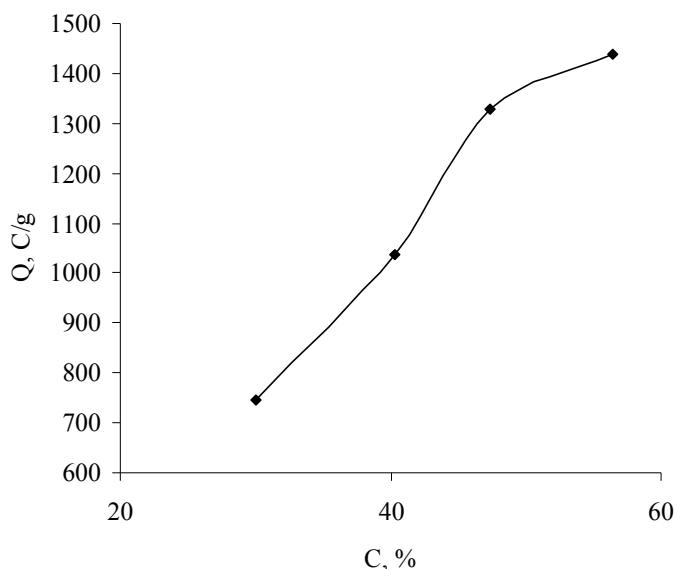


Fig. 10. Dependence of the maximum specific charge of CH900-20 on the sulfuric acid concentration for the charging time of 18 h.

According to Faraday's law, formation of compound C_6H requires 1320 C/g. The maximum value of $Q_{max} = 1560$ C/g was obtained in our investigation. Therefore, other rechargeable processes require 240 C/g. This value includes in the first instance the value of $Q_{EDL} = C_{EDL} \times \Delta E$, where ΔE is the range of potentials. In this case, $\Delta E = 1.4$ V, so to the first approximation, $C_{EDL} = 240/1.4 = 170$ F/g. This is approximately the same value as the one obtained from curve 4 in Fig. 3. It must be noted that, this is an approximate estimate, as the C_{EDL} value somewhat depends on the potential and also as a small contribution into the Q_{max} value is made by the pseudocapacitance of redox reactions of surface groups. Nevertheless, this approximate estimate shows the correctness of the assumed mechanism of deep AC charging. Though the process of electrochemical chemisorption on the carbon/electrolyte

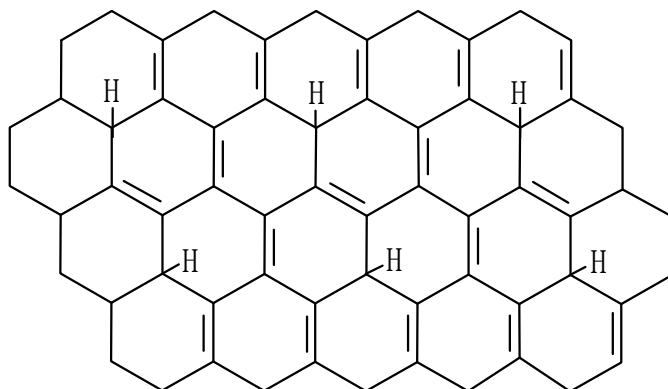


Fig. 11. Structural formula of compound C₆H.

interface and the bulk process of hydrogen intercalation occur at different rates, both of them eventually lead to formation of the single bulk compound C₆H.

Fig. 12 presents the obtained dependence of Q on the charging potential. It can be seen that the curve reaches a plateau at $E < -250$ mV. The very fact of reaching a plateau points to a saturation of the carbon bulk and surface by hydrogen atoms, i.e., evidences indirectly the saturation of the C_x-H chemical bonds at the given potential and H₂SO₄ concentration.

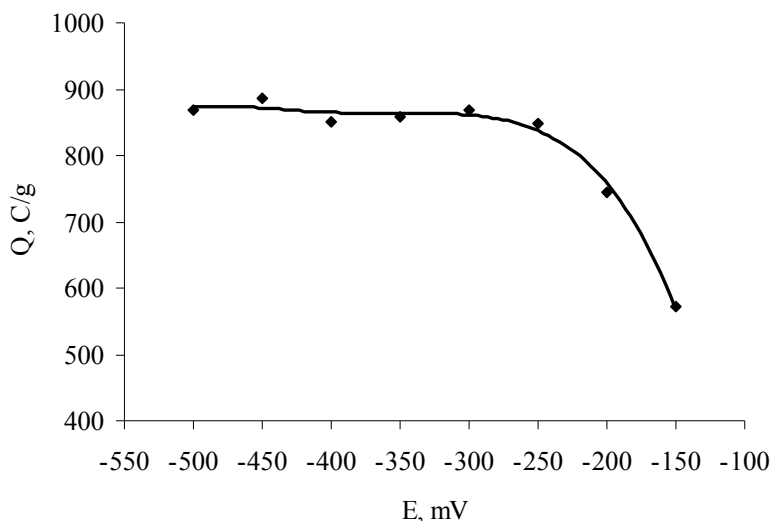


Fig. 12. Dependence of specific capacitance on the potential of charging for 18 h in 40.3% H₂SO₄.

Thus, neither the further increase in the concentration of H₂SO₄ above 56.4%, nor the further decrease in the charging potential below -250 mV, nor any increase in the charging time result in an increase in the maximum specific charge $Q_{\max} = 1560$ C/g. As pointed out above,

the contribution into this DEL capacitance value is 240 C/g, so the dominating contribution to the Q_{\max} value is made by the specific charge $Q = 1320$ C/g corresponding to formation of the C_6H compound (pseudocapacitance charge). In principle, if one uses other activated carbons and cloths, the DEL capacitance value may somewhat increase due to an increase in the AC specific surface area that in our case was 1520 m²/g. However, this must not result in any significant increase in the Q_{\max} value.

Fig. 13 shows an impedance Cole-Cole plot (capacitive impedance component vs. resistive component) for an activated carbon electrode in a 30% sulfuric acid solution at $E=0.430$ V measured in the frequency range from 100 kHz to 0.01 GHz. In this figure also shown is a fitting plot calculated from the staircase-type equivalent circuit shown in Fig. 14. Such a circuit-type is often used for EDLC electrodes [1]. We interpret this circuit by the simultaneous proceeding of different events: DL-charging, redox-reactions of different surface groups, hydrogen chemisorption and hydrogen intercalation. As the size of micropores is comparable to the DL- thickness, the DL capacity and the kinetic parameters of surface-group reactions can vary for pores of different size. Each of these processes has its own "stairstep" in the equivalent circuit. The absence in this circuit of a Warburg impedance, corresponding to a hydrogen diffusion in the solid phase, can be explained by the time constants of such a diffusion being much higher than the lowest frequencies (0.01 Hz) which can be used for such measurements.

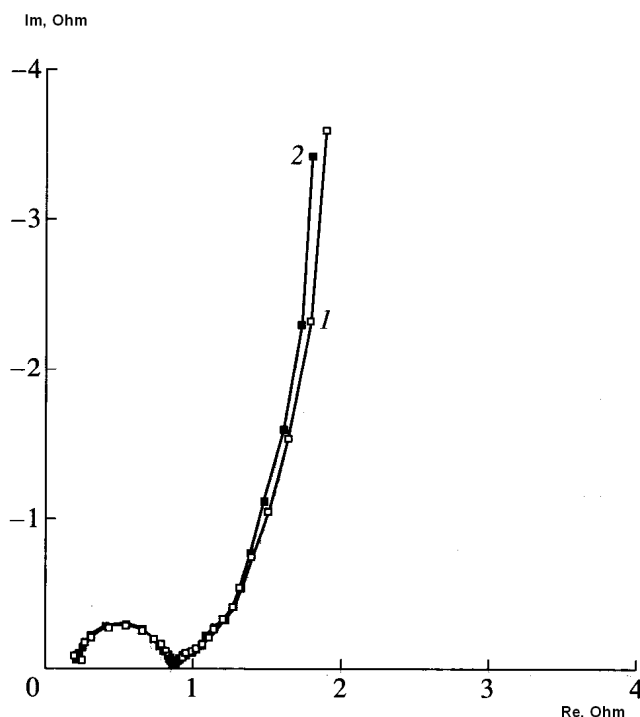
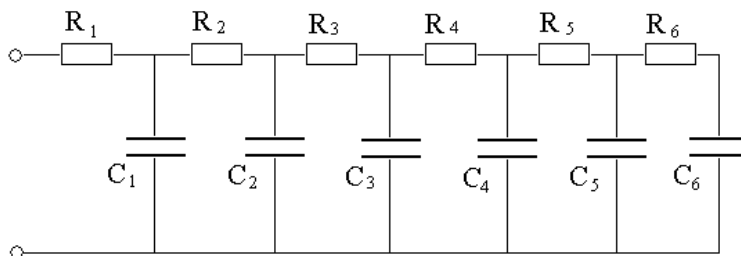


Fig. 13. Impedance plot for an activated carbon electrode in a 30% sulfuric acid solution at $E=0.430$ V



N	1	2	3	4	5	6
R, Ohm	0.29	1.99	1.2	0.57	2.22	2.86
C, F	$3.2 \cdot 10^{-5}$	1.41	3.43	$8.2 \cdot 10^{-2}$	$4.0 \cdot 10^{-3}$	$4.4 \cdot 10^{-5}$

Fig. 14. Equivalent circuit fitting the plot on Fig. 13, the values of the circuit's components are presented in the table below the figure

Galvanostatic cycling of the CH900-20 electrode was carried out at the current density of 1.2 mA/cm² in the range of potentials from -0.32 V to 1.03 V. Fig. 15 presents the dependence of specific discharge capacitance Q on number of cycles N. One may see that the Q value changed little in 100 cycles. Then the cycling was stopped, as it had already taken a lot of time: 588 h. The mean Q value was 940 C/g. At N = 100, the obtained overall discharge capacitance was 26.3 A h/g. Fig. 16 presents cyclic charge-discharge curves for 8 cycles. The difference between these curves and the ideal "sawtooth" is related to occurrence of the above pseudocapacitance processes.

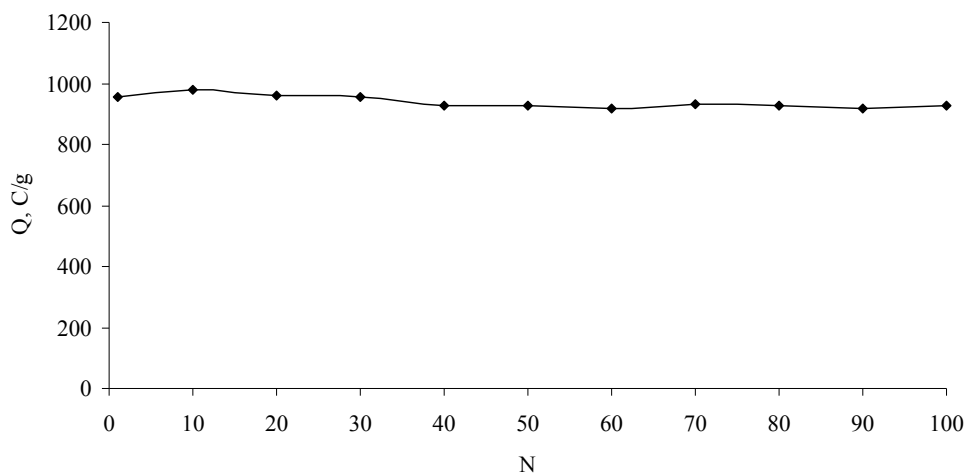


Fig. 15. Dependence of specific discharge capacitance Q on the number of cycles.

Besides the measurements of deep cathodic charging of CH900-20 ACC in H₂SO₄ solutions, similar measurements were carried out in a 90% aqueous H₃PO₄ solution. The specific charge value calculated using this plot was 1200 C/g. As according to [37], phosphoric acid is also intercalated into graphite and graphite-like compounds, these results agree with the

above mechanism of double intercalation of H_3PO_4 and hydrogen into AC carbon during deep cathodic charging.

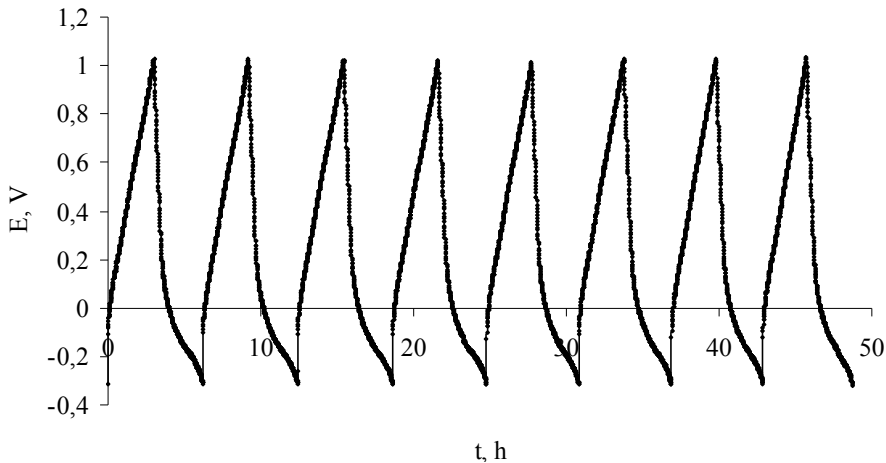


Fig. 16. Cyclic charging–discharge curves for 8 cycles.

The above data point to high prospects of using ACs under the conditions of deep cathodic charging for energy type supercapacitors.

4. Mathematic charging–discharge model of electrode based on activated carbon

We developed a two-dimensional mathematical model of charging–discharge for highly dispersed carbon accounting for the obtained experimental results.

Hydrogen solid-phase diffusion may be assumed to be one-dimensional due to strong anisotropy of carbon crystallites forming the porous structure, as there is practically no diffusion in transverse direction to graphene layers [40]. Then the equation for hydrogen diffusion for crystallites may be written in a one-dimensional form:

$$\frac{\partial c}{\partial t} = D \frac{\partial^2 c}{\partial x^2}, \quad (3)$$

where c is the hydrogen concentration in the AC carbon, t is the time, x is the shortest axial coordinate of the crystallite, D is the longitudinal solid-phase diffusion coefficient of hydrogen in the crystallite. The boundary condition at the interface of carbon/electrolyte in pores is:

$$i_p = nFD \left. \frac{\partial c}{\partial x} \right|_{x=0}, \quad (4)$$

where n is the charge transferred, F is Faraday's number, i_p is the current density determined by the kinetic dependence of the reaction. Let us also assume that there is a certain length H corresponding to half the crystallite length, where there is no hydrogen diffusion flux due to the symmetry:

$$0 = \left. \frac{\partial c}{\partial x} \right|_{x=H} \quad (5)$$

The intercalation current density is determined by the Butler-Volmer kinetics:

$$i_i(\eta) = i_0 \left(\frac{c}{c_0} e^{\frac{\alpha\eta F}{RT}} - \frac{c - c_H}{c_0} e^{-\frac{(1-\alpha)\eta F}{RT}} \right) \quad (6)$$

where i_0 is the exchange current density, c_0 is the hydrogen concentration at the interface, α is the electrochemical reaction transfer coefficient. Let us assume that the initial state of the discharge process is saturation of carbon by hydrogen; then the initial condition for equation (2) is:

$$c = c_H \Big|_{t=0} \quad (7)$$

Apart from the current density described in (4), there is also hydrogen adsorption current and double electric layer (DEL) charging current in the system. Let us assume that the hydrogen adsorption current is determined by Temkin's adsorption equation [40]:

$$i_A(\eta, \theta) = i_{0A} \left(e^{\frac{\alpha_1 s_T (\theta - 0.5)}{2}} e^{\frac{\alpha_1 \eta F}{RT}} - e^{-\frac{(1-\alpha_1)\eta F}{RT}} e^{\frac{s_T (1-\alpha_1)(\theta - 0.5)}{2}} \right), \quad (8)$$

where i_{0A} is the adsorption exchange current density, θ is the surface coverage, α_T is the adsorption transfer coefficient, s_T is the adsorption heat decrease coefficient, K_0 is the adsorption constant, c_H is the concentration of hydrogen ions in electrolyte. Coverage and adsorption current are connected through the following relationship:

$$\frac{\partial \theta}{\partial t} = \frac{i_A}{q_1} \quad (9)$$

where q_1 is the full potential adsorption capacitance. The DEL capacitance current may be written as:

$$i_{EDL} = C_{EDL} \frac{\partial \eta}{\partial \tau} \quad (10)$$

where η is the potential. Intercalation, adsorption, and EDL charging currents are included into the equation determining the polarization distribution across the porous electrode thickness that may be presented as:

$$\frac{\partial}{\partial y} \left(\kappa \frac{\partial \eta}{\partial y} \right) = \gamma s i_i + s i_{EDL} + s i_A \quad (11)$$

where κ is the conductivity of electrolyte in the pores determined according to the Archie relationship: $\kappa = \kappa_0 \varepsilon^2$ [41], s is the specific surface area, ε is the porosity, γ is the ratio of half the mean thickness of walls between pores l and value H . It was assumed in equation (9) that specific conductivity of the carbon material is much higher than conductivity of electrolyte. The H value may be provisionally determined on the basis of the literature on activated carbons

[38]: $l \sim 1/s\rho$, where ρ is the carbon density in activated carbons. $\rho \sim 2 \text{ g/cm}^3$. Assuming that $s = 10^7 \text{ cm}^2/\text{g}$, $l \sim 0.5 \text{ nm}$. The H value is approximately 50 nm. Therefore, $\gamma \sim 0.01$.

If the adsorption rate is much higher than the rate of hydrogen solid-phase diffusion (as in our case), then the nonsteady-state charging process is described by equation (12):

$$\frac{\partial}{\partial y} \left(\kappa \frac{\partial \eta}{\partial y} \right) = \gamma s i_i + (s C_{EDL} + s C_A) \frac{\partial \eta}{\partial \tau} \quad (12)$$

where C_A is the hydrogen concentration at the interface. In the case of the galvanostatic mode, the boundary conditions for equation (10) are written as:

$$\kappa \cdot \frac{\partial \eta}{\partial y} \Big|_{y=0} = 0, -\kappa \cdot \frac{\partial \eta}{\partial y} \Big|_{y=L} = I, \quad (13)$$

where L is the porous electrode thickness. I is the overall current density per electrode unit visible surface.

The system of equations (3)–(13) is the system with parameters twice distributed along the x and y axes; it describes hydrogen intercalation and adsorption in the porous carbon structure and also EDL charging.

This system of equations was solved numerically using the COMSOL Multiphysics FemLab3.5 software package.

The fitting yielded better convergence of these curves for the set of system parameters presented in Table 1 as followed from the comparison of calculated and experimental galvanostatic discharge curves.

Parameters, [dimension]	Values
α, α_1 are the transfer coefficients	0.5
D is the hydrogen solid-phase diffusion coefficient, [cm^2/s]	10^{-14}
H is the crystallite half-length, [cm]	4×10^{-6}
L is the electrode thickness, [cm]	0.05
i_0 is the exchange current density of hydrogen intercalation, [A/cm^2]	$0.5 \cdot 10^{-8}$
i_{0A} is the exchange current density of hydrogen adsorption, [A/cm^2]	$>10^{-6}$
γ is the crystallite shape factor	0.01
C_{EDL} is the DEL specific capacitance, [F/cm^2]	1.84×10^{-5}
S_{phi} is the specific hydrophilic surface, [cm^{-1}]	0.87×10^7
ϵ is the porosity	0.86
Q_1 is the maximum adsorption charge capacitance, [C/cm]	$1.3 \cdot 10^{-5}$
s_T is the adsorption heat decrease coefficient	40
c_H is the limiting concentration of protons in carbon, [m/cm^3]	1 / 74
T is the system temperature, [K^0]	298
κ is the specific conductivity of electrolyte, [S/cm]	0.1
I is the overall current density per unit visible surface, [A/cm^2]	0.0020

Table 1. System parameters used for calculation

Herewith, most of the parameters were taken from the experiment. The parameters obtained as a result of simulation are as follows: D , i_0 , q_1 , i_{0A} . It was assumed in the calculations that the slowest process is hydrogen solid-phase diffusion (fast adsorption).

Fig. 17 presents the results of simulation of the galvanostatic discharge curve (dependence of the potential on the discharge time) at the current density of 2 mA/cm^2 .

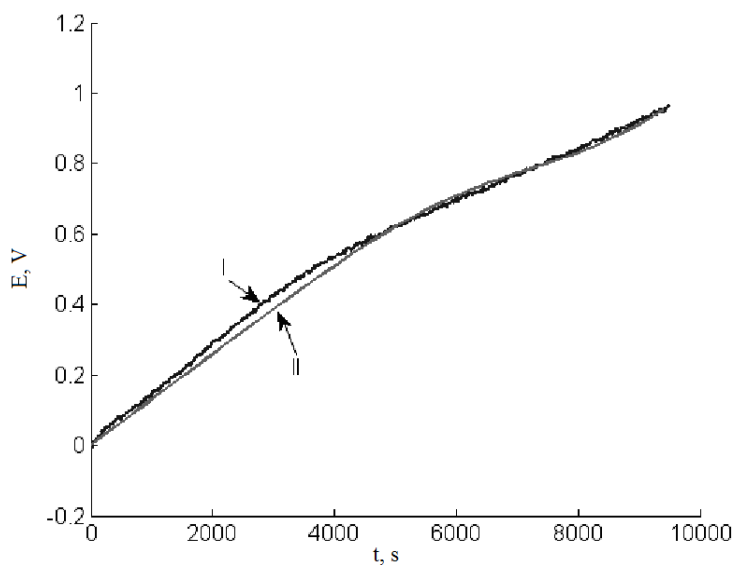


Fig. 17. Fitting of the discharge curve for the current density of 2 mA/cm^2 . (I) The experimental curve, (II) the calculated curve.

This figure shows good agreement between the calculated and experimental curves, which evidences the correction of the model assumed.

The fitting yielded an approximate value of hydrogen solid-phase diffusion coefficient into AC carbon $D \sim 10^{-14} \text{ cm}^2/\text{s}$.

Fig. 18 presents the distribution (profile) of dimensionless concentration at the end of discharge by two coordinates, x and y . One may see thence that nonuniform hydrogen concentration distribution, by both coordinates, x and y , occurs at the given system parameters.

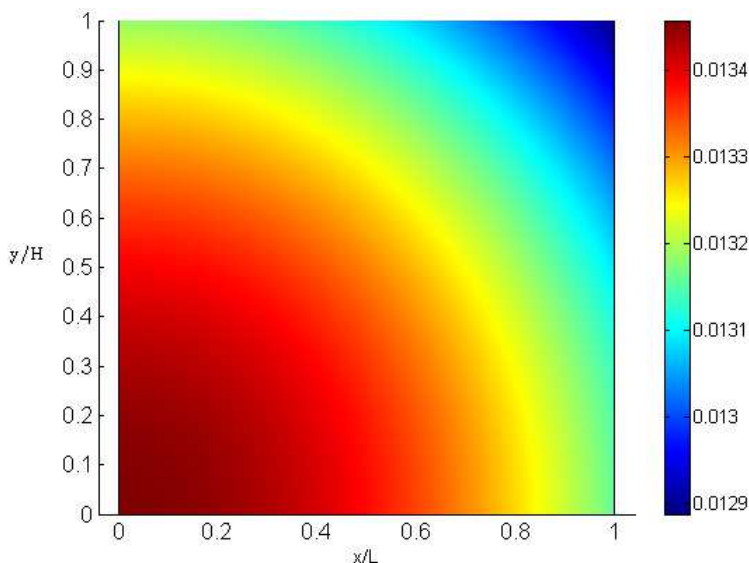


Fig. 18. Dimensionless concentration profile at the end of discharge.

5. Conclusion

Electrochemical properties of electrodes based on CH900-20 activated carbon (AC) cloth were studied in concentrated H_2SO_4 solutions in a wide range of potentials from -0.8 to $+1$ V RHE. Cyclic voltammetric curves measured in two ranges of potential were studied: in the reversibility range (from 0.1 to 0.9 V) and in the deep cathodic charging range (from -0.8 to $+1$ V). Electric double electric layer (EDL) charging occurs in the reversibility range, while faradaic processes of hydrogen chemisorption (at the interface of carbon and electrolyte in pores) and its intercalation into AC carbon takes place in the range of negative potentials (< -0.1 V). The intercalation process is controlled by slow solid-phase hydrogen diffusion into AC carbon. For the first time, the maximum value of specific discharge capacitance of 1560 C/g was obtained, which is much higher than the values known from the literature for carbon electrodes. On the basis of this value and Faraday's law, it was assumed that the compound of C_6H is formed in the limiting case of AC deep cathodic charging. The specific charge value grows at an increase in the concentration of H_2SO_4 and also at an increase in the charging time.

The obtained experimental data were interpreted by a mechanism of double intercalation under AC deep cathodic charging. Sulfuric acid is intercalated into AC expanding the interlayer (intergraphene) space. Hydrogen atoms are then directed into this space. This interlayer space serves as a transport route for hydrogen. Then hydrogen interacts with graphene layers with formation in the limit of compound C_6H . The data obtained were used to develop a mathematical charging–discharge model for an AC electrode taking into account the EDL charging, chemisorption, and hydrogen intercalation.

The data obtained in this work according to which at deep cathodic charging of activated carbon based electrodes to potential values from -0.1 to -0.5 V RHE very high discharge capacities can be achieved point to high prospects of such a use of these electrodes in energy type supercapacitors. At the same time they allow to explain the high specific energy values (up to 20 Wh/kg) observed ten years ago for hybrid (+)PbO₂/H₂S₄/AC(-) supercapacitors [17,18]. These high values were achieved at a maximal charging voltage U_{\max} of 2.2 V. Taking into account that for the positive PbO₂ electrode $E^+_{\max} = 1.85$ V RHE and therefore the value of E^-_{\min} was -0.35 V RHE corresponding to the region of maximal capacity for activated carbon based electrodes.

6. References

- [1] B.E. Conway. Electrochemical supercapacitors. Kluwer Academic / Plenum Publishers, New York. 1999. 698 p.
- [2] Yu.M. Volkovich, T.M. Serdyuk. Russ. J. Electrochem. 38 (2002) 935.
- [3] I.V. Barsukov, C. Johnson, E. Doninger, V.Z. Barsukov, New Carbon Based Materials for Electrochemical Energy Storage Systems: Batteries, Supercapacitors and Fuel Cells (NATO Science Series II: Mathematics, Physics and Chemistry), Springer, NY, 2006. 297 p.
- [4] R. Kotz, M. Carlen. Electrochimica Acta 45 (2000) 2483.
- [5] A.G. Pandolfo, A.F. Hollenkamp. J. Power Sources 157 (2006) 11.
- [6] P. Simon, Y. Gogotsi. Nature Materials 7 (2008) 845.
- [7] Y. Chen, X. Zhang, P. Yu, Y. Ma. J. Power Sources 195 (2010) 3031.
- [8] Y. Chen, X. Zhang, D. Zhang, P. Yu, Y. Ma. Carbon 49 (2011) 573.
- [9] W. Lu, L. Qu, K. Henry, L. Dai. J. Power Sources 189 (2009) 1270.
- [10] M.D. Stoller, S. Park, Z. Yanwu, J. An, R.S. Ruoff. Nano Letters 8 (2008) 3498.
- [11] R.C. Vivekchand, C.S. Rout, K.S. Subrahmanyam, A. Govindaraj, C.N.R. Rao. J. Chem. Sci. 120 (2008) 9.
- [12] H. Zhang, G. Cao, Y. Yang, Z. Gu. J. Electrochem. Soc. 155 (2008) K.19.
- [13] B.P. Bakhmatyuk, B.Y. Venhryn, I.I. Grygorchak, M.M. Micov, Y. Kulyk. Electrochimica Acta 52 (2007) 6604.
- [14] S. Lidorenko. Doklady Akademii Nauk USSR . 216 (1974) 1261.
- [15] A.I. Beliakov., A.M. Brintsev. Proc. 7th Int. Seminar on Double Layer Capacitors and Similar Energy Storage Devices. Deerfield Beach. Florida. 1997. V. 7.
- [16] A.I. Beliakov. Proc. 8th Int. Seminar on Double Layer Capacitors and Similar Energy Storage Devices. Deerfield Beach. Florida. 1998. V. 8.
- [17] Belyakov, Yu.M. Volkovich, P.A. Shmatko at al. US Patent 6,195,252 B1 (2001).
- [18] Yu.M. Volkovich, P.A. Shmatko. US Patent 6,628,504 (2003).

- [19] J. P. Zheng, S. P. Ding, T. R. Jow. Proc. 7th Int. Seminar on Double Layer Capacitors and Similar Energy Storage Devices. Deerfield Beach. Florida. 1997.
- [20] B. Fang, L. Binder. *J. Power Sources*, 163 (2006) 616.
- [21] T. Centeno, F. Stoeckli, *Electrochimica Acta* 52 (2006) 560.
- [22] M.J. Bleda-Martinez, J.A. I. Agull, D. Lozano-Caste, E. Morall, D. Cazorla-Amor, A. Linares-Solano. *Carbon* 43 (2005) 2677.
- [23] Yu.M. Volkovich, A.Yu. Rychagov, V.E.Sosenkin, A.V. Krestinin. *Elektrokhimicheskaya Energetika*. 8 (2008) 106.
- [24] M.Yu. Izmailova, A.Yu. Rychagov, K.K. Den'shchikov, Yu.M. Volkovich, Ya.S. Vygodskii, E.I. Lozinskaya. *Russ. J. Electrochem.*, 45 (2009) 949.
- [25] A.Yu. Rychagov, Yu.M. Volkovich. *Russ. J. Electrochem.*, 45 (2009) 304.
- [26] Yu.M. Volkovich, V.M. Mazin, N.A. Urisson. *Russ. J. Electrochem.*, 34 (1998) 740.
- [27] Yu.M. Volkovich, O.A. Petrii, A.A. Zaitsev, I.V. Kovrigina, *Vestnik MGU. Ser. 2, Khimiya*. 29 (1988) 173.
- [28] Yu. M. Volkovich, V. S. Bagotzky, T. K. Zolotova and E. Yu. Pisarevskaya. *Electrochimica Acta* 41 (1996) 1905.
- [29] Yu. M. Volkovich, A. G. Sergeev, T. K. Zolotova, S.D. Afanasiev, O.N. Efimov, E.P. Krinichnaya. *Electrochimica Acta*, 44 (1999) 1543.
- [30] S. Fernandez, E.B. Cartro, S.G. Real, M.E. Martines. *Internat. J. Hydrogen Energy*, 34 (2009) 8115.
- [31] B.P. Bakhmatyuk, B.Ya. Venhryn, I.I. Grigorochak, m.M. Micov, Yu.O.Kulik. *Electrochimica Acta*, 52 (2007) 6604.
- [32] Yu.M. Volkovich, V.S. Bagotzky, V.E. Sosenkin, I.A. Blinov. In: *Colloid and Surfaces A: Physicochemical and Engineering Aspects*. 187-188 (2001) 349.
- [33] A.N. Frumkin, V.S. Bagotskii, Z.A. Iofa, B.N. Kabanov. *Kinetika elektrodnykh protsessov (Kinetics of Electrode Processes)*. Moscow: Izd. MSU, 1952.
- [34] M.R. Tarasevich. *Elektrokhimiya uglerodnykh materialov (Electrochemistry of Carbon Materials)*. Moscow.: Nauka. 1984. P. 251.
- [35] A.R. Ubellode, F.A. L'yuis. *Grafit I ego kristallicheskie soedineniya (Graphite and Its Crystalline Compounds)*. Moscow: Mir, 1965. 256 pp.
- [36] A.S. Fialkov. *Uglerod, mezhslouevye soedineniya i kompozity na ego osnove (Carbon, Interlayer Compounds and Composites on Its Basis)*. Moscow: Aspect press, 1997.
- [37] N.E. Sorokina, I.V. Nikol'skaya, S.G. Ionov, V.V. Avdeev, *Izv RAS, Ser. Khim.* 54 (2005) 1.
- [38] V. Yu. Yakovlev, A.A.Fomkin, A.V. Tvardovski. *J. Colloid Interface Sci.* 280 (2004) 305.
- [39] A.Yu. Rychagov, N.A. Urisson, Yu.M. Volkovich. *Russ. J. Electrochem.* 37 (2001) 1172.
- [40] A.Yu. Rychagov, Yu.M. Volkovich, *Russ.J. Electrochem.*, 43 (2007) 1343.
- [41] V.B. Fenelonov. *Poristy uglerod (Porous Carbon)*. Novosibirsk. 1995.
- [42] P. Delahay. *Double layer and electrode kinetics*. John Wiley & sons, Inc., New York. 1965. 340 p.

- [43] Yu.A. Chizmadzhev, V.S. Markin, M.R. Tarasevich, Yu.G. Chirkov. Makrokinetika protsessov v poristyykh sredakh (Macrokinetics of Processes in Porous Media). Moscow: Nauka, 1971. 364 p.



Recent Trend in Electrochemical Science and Technology

Edited by Dr. Ujjal Kumar Sur

ISBN 978-953-307-830-4

Hard cover, 306 pages

Publisher InTech

Published online 27, January, 2012

Published in print edition January, 2012

This book titled "Recent Trend in Electrochemical Science and Technology" contains a selection of chapters focused on advanced methods used in the research area of electrochemical science and technologies; descriptions of electrochemical systems; processing of novel materials and mechanisms relevant for their operation. This book provides an overview on some of the recent development in electrochemical science and technology. Particular emphasis is given both to the theoretical and the experimental aspect of modern electrochemistry. Since it was impossible to cover the rich diversity of electrochemical techniques and applications in a single issue, the focus is on the recent trends and achievements related to electrochemical science and technology.

How to reference

In order to correctly reference this scholarly work, feel free to copy and paste the following:

Yu.M. Volfkovich, A.A. Mikhailin, D.A. Bograchev, V.E. Sosenkin and V.S. Bagotsky (2012). Studies of Supercapacitor Carbon Electrodes with High Pseudocapacitance, Recent Trend in Electrochemical Science and Technology, Dr. Ujjal Kumar Sur (Ed.), ISBN: 978-953-307-830-4, InTech, Available from: <http://www.intechopen.com/books/recent-trend-in-electrochemical-science-and-technology/studies-of-supercapacitor-carbon-elrctrodes-with-high-pseocapacitance>

INTECH

open science | open minds

InTech Europe

University Campus STeP Ri
Slavka Krautzeka 83/A
51000 Rijeka, Croatia
Phone: +385 (51) 770 447
Fax: +385 (51) 686 166
www.intechopen.com

InTech China

Unit 405, Office Block, Hotel Equatorial Shanghai
No.65, Yan An Road (West), Shanghai, 200040, China
中国上海市延安西路65号上海国际贵都大饭店办公楼405单元
Phone: +86-21-62489820
Fax: +86-21-62489821

© 2012 The Author(s). Licensee IntechOpen. This is an open access article distributed under the terms of the [Creative Commons Attribution 3.0 License](#), which permits unrestricted use, distribution, and reproduction in any medium, provided the original work is properly cited.